PHYSICAL REVIEW C VOLUME 31, NUMBER 1 JANUARY 1985

# Proton stripping to outer subshells and the damping of single-particle states: $^{116}$Sn, $^{144}$Sm, and $^{208}$Pb($\alpha$,t) reactions at 80 MeV

S. Gales, C. P. Massolo, S. Fortier, and J. P. Schapira
*Institut de Physique Nucleaire, 91406 Orsay Cedex, France*

P. Martin and V. Comparat
*Institut des Sciences Nucleaires, 38026 Grenoble Cedex, France*
(Received 15 August 1984)

The stripping reaction ($\alpha$,t) at 80 MeV incident energy has been used to study the proton-particle response function on $^{116}$Sn, $^{144}$Sm, and $^{208}$Pb target nuclei up to 22 MeV excitation energy. Rather complete spectroscopic information has been obtained on the low-lying proton states (0—3 MeV) through angular distribution measurements and standard distorted wave Born approximation analysis. Strong transitions to high-lying proton states located between 5 and 12 MeV excitation energy in $^{145}$Eu and $^{209}$Bi are observed whereas the spectrum from the $^{116}$Sn($\alpha$,t) reaction displays only broad, weak enhancement of cross sections at high excitation. These transitions appear as broad bumps superimposed on a continuous background for which a qualitative analysis within the framework of the breakup model has been attempted. The excitation energies, angular distributions, and strengths of these high-lying transitions suggest that they arise from proton stripping to high-spin outer subshells, e.g., $1h\frac{9}{2}$ and $1i\frac{13}{2}$ in $^{145}$Eu, and $1i\frac{11}{2}$ and $1j\frac{15}{2}$ in $^{209}$Bi. A distorted-wave Born approximation analysis using resonant form factors for the states located above the proton threshold has been carried out. The deduced proton strength distributions are compared with the predictions from the quasiparticle-phonon and single-particle vibration coupling nuclear models. Around 12—14 MeV excitation energy, narrow peaks corresponding to the population of the isobaric analog states in $^{117}$Sb and $^{145}$Eu are also observed. Our results are compared to the known spectroscopic properties of the corresponding parent states in $^{117}$Sn and $^{145}$Sm.

## I. INTRODUCTION

With the exception of the well-known studies of proton stripping to quasibound or unbound isobaric analog states (IAS),[1,2] practically no information is available on high-lying particle states in medium weight and heavy nuclei.[3] During the past few years, systematic studies of the neutron-hole response function have been carried out using pickup reactions[4] and valuable information has been obtained on the characteristics of deeply-bound hole states in heavy nuclei. The theoretical models developed to explain the empirical systematics suggest that the hole states mix extensively with both low- and high-lying phonon states,[5—7] and a similar situation is expected for the particle states located well above the Fermi level. Moreover, in the case of the particle states, an additional term contributes to the spreading width via a direct coupling to the continuum states. Therefore, experimental data on the characteristics of particle states via transfer reactions and the exploration of a very large excitation energy range with good energy resolution are highly desirable.

In a recent paper, the first observation of high-lying proton strengths in $^{145}$Eu populated through a stripping reaction has been reported.[8] Two broad bumps located at 5.9 and 7.6 MeV dominate the high energy part of the residual spectrum. These features display striking similarities with those observed in the early experiments on deeply-bound states in the Sn isotopes.[3,4,9] The analysis of the data has shown that such broad "peaks" arise from proton stripping to high-spin orbitals (here $1h\frac{9}{2}$ and $1i\frac{13}{2}$) belonging to the next major shells ($Z>82$). In close connection with the properties of the neutron pickup process at high incident energy, it was demonstrated that the ($\alpha$,t) or ($^3$He,d) reactions are well suited to the investigation of high-spin particle states due to their known selectivity for large $l$ transfers.

In this paper, we present the result of a study of the ($\alpha$,t) reaction at $E_\alpha=80$ MeV on $^{116}$Sn, $^{144}$Sm, and $^{208}$Pb targets, chosen because their proton numbers range from $Z=50$ to 82. Along with the location of outer subshells, detailed information has been obtained on valence-particle state fragmentation. The results of our analysis for the low-lying states will be presented in Sec. III and compared to previous investigations.

## II. EXPERIMENTAL METHOD

The experiments were performed with the $K$90 isochronous Institut de Physique Nucleaire (ISN) Grenoble cyclotron. An energy-analyzed beam of 80 MeV alpha particles was incident upon self-supporting metallic foils of $^{116}$Sn, $^{144}$Sm, and $^{208}$Pb. Two different sets of targets were used during the experiments. Their thicknesses and isotopic enrichments are listed in Table I. We obtained a current of 50 nA on target and the collected charge was measured in a Faraday cup. The outgoing tritons were momentum analyzed by the quadrupole-dipole (QD) magnetic spectrometer. Their position on the focal plane was

 

TABLE I. Characteristics of the targets used in the study of the (α,t) reactions.

| Isotopes | Thickness (mg/cm²) | Enrichment (%) | $Q_{\text{value}}$[a] (α,t) (MeV) |
|---|---|---|---|
| $^{116}$Sn (thin) | 2.1 | 98 | −15.410 |
| $^{116}$Sn (thick) | 6 | 98 | |
| $^{144}$Sm (thick) | 6 | 96 | −16.550 |
| $^{144}$Sm (thin) | 0.3 | 96 | |
| $^{208}$Pb (thick) | 6 | 98 | −16.010 |
| $^{208}$Pb (thin) | 1 | 98 | |

[a]Reference 10.

measured using a gas delay-line counter backed by two plastic scintillators. Due to the high magnetic rigidity of the triton particles, a clean particle identification could be accomplished by a time-of-flight measurement (between the rf of the cyclotron and the plastic detector). The solid angle of the spectrometer was 1 msr. The absolute cross sections were determined using the known values of the target thicknesses and of the spectrometer solid angle. The error in the absolute cross-section scales is estimated to be of the order of ±10%. An excitation energy range of 22 MeV has been explored using two successive exposures at different magnetic fields. We obtained an overall

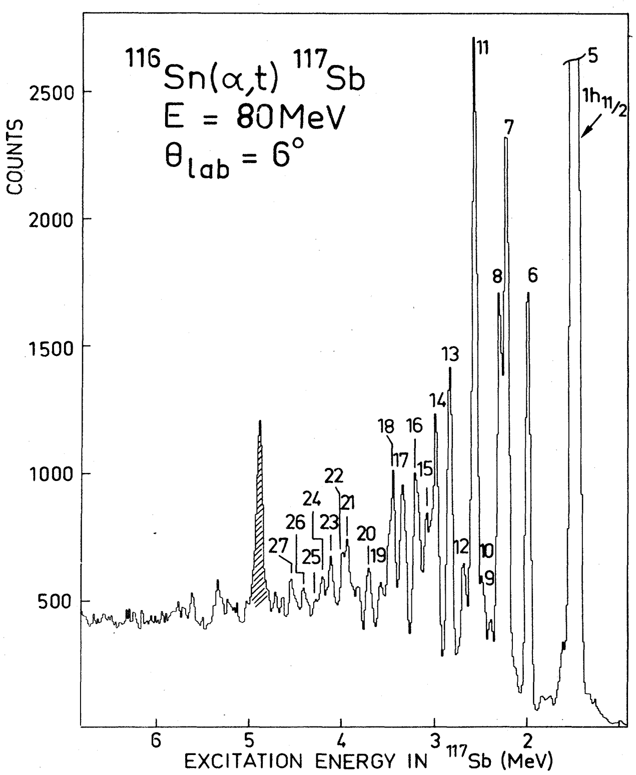


FIG. 1. Alpha particles energy spectrum from the $^{116}$Sn(α,t)$^{117}$Sb reaction. The numbers at the top of the peaks refer to $^{117}$Sb levels. They are listed in Table II. The horizontal scale indicates the excitation energy in the $^{117}$Sb nuclei. Hatched peaks originate from the (α,t) reaction on $^{12}$C and $^{16}$O impurities present in the target.

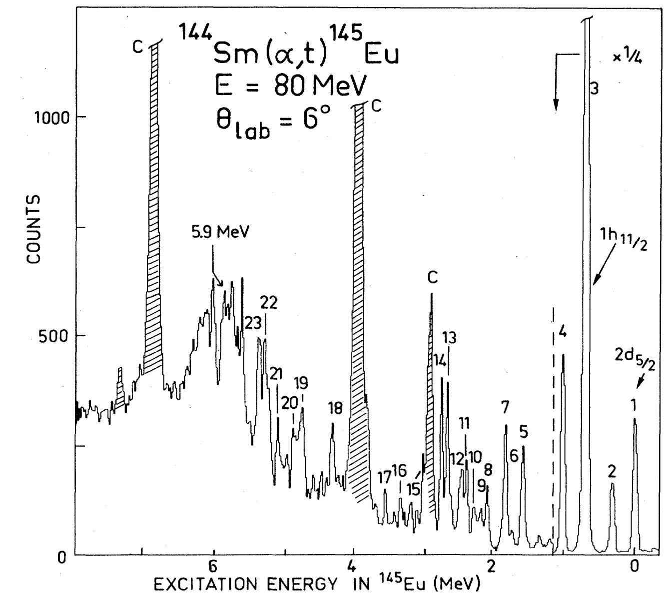


FIG. 2. Same as in Fig. 1 for the $^{144}$Sm(α,t)$^{145}$Eu reaction (see Table III).

energy resolution of 60 keV with thin $^{116}$Sn, $^{144}$Sm, and $^{208}$Pb targets. With the thicker ones the energy resolution was limited to 200 keV.

An accurate energy calibration of the counter was obtained by using the known energies of the low-lying states in the $^{145}$Eu and $^{209}$Bi nuclei and some strong lines from proton stripping reactions on $^{12}$C and $^{16}$O contaminants present in the target. Angular distributions have been measured for the three nuclei investigated here from 1.75° to 21° laboratory angle typically in 3° steps.

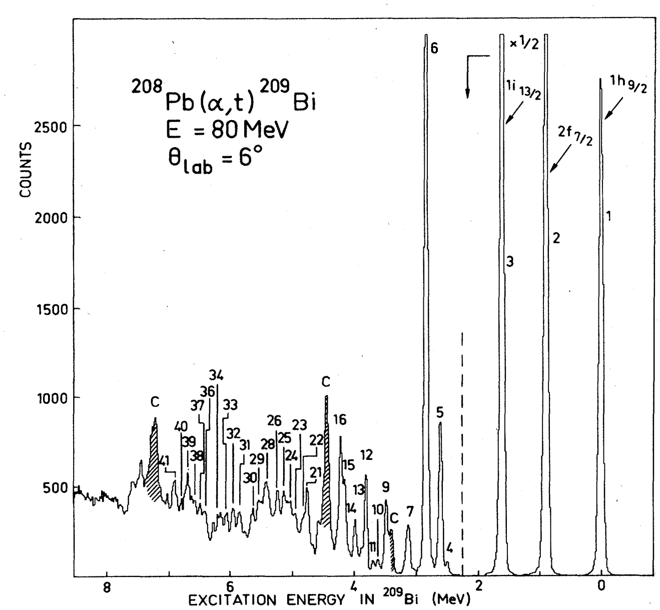


FIG. 3. Same as in Figs. 1 and 2 for the $^{208}$Pb(α,t)$^{209}$Bi reaction (see Table IV).

TABLE II. Results from the analysis of the $^{116}Sn(\alpha,t)$ reaction to low-lying states (0—4 MeV).

| No. | $E_x$ (MeV) | $l$ | $J^\pi$ | $C^2S$ | $C^2S$ [a] Other works |
|---|---|---|---|---|---|
| 1 | 0.00 | 2 | $\frac{5}{2}^+$ | | 0.85—0.70 |
| 2 | 0.520 | 4 | $\frac{7}{2}^+$ | 0.64 | 0.80—0.70 |
| 3 | 0.720 | 0 | $\frac{1}{2}^+$ | | 1.2—0.6 |
| 4 | 0.920 | 2 | $\frac{3}{2}^+$ | 0.35 | 0.49—0.42 |
| 5 | 1.311 | 5 | $\frac{11}{2}^-$ | 0.42 | 0.52—0.45 |
| 6 | 1.865 | 4 | $(\frac{7}{2})^+$ | 0.14 | |
| 6′ | 2.012 | 2 | $(\frac{3}{2})^+$ | 0.03 | |
| 7 | 2.112 | 5 | $(\frac{11}{2})^-$ | 0.06 | |
| 8 | 2.195 | 4 | $(\frac{7}{2})^+$ | 0.16 | |
| 9 | 2.305 | 5 | $(\frac{11}{2})^-$ | 0.01 | |
| 10 | 2.397 | 2 | $(\frac{3}{2})^+$ | 0.05 | |
| 11 | 2.485 | 5 | $(\frac{11}{2})^+$ | 0.06 | |
| 12 | 2.604 | 4 | $(\frac{7}{2})^+$ | 0.05 | |
| 13 | 2.771 | 5 | $(\frac{11}{2})^-$ | 0.03 | |
| 14 | 2.936 | 5 | $(\frac{11}{2})^-$ | 0.03 | |
| 15 | 3.039 | 5 | $(\frac{11}{2})^-$ | 0.02 | |
| 16 | 3.158 | 6 | $(\frac{13}{2})^+$ | 0.02 | |
| 17 | 3.313 | 5 | $(\frac{11}{2})^-$ | 0.02 | |
| 18 | 3.442 | 6 | $(\frac{13}{2})^+$ | 0.02 | |
| 19 | 3.550 | 5 | $(\frac{11}{2})^-$ | 0.01 | |
| 20 | 3.702 | 5 | $(\frac{11}{2})^-$ | 0.01 | |
| 21 | 3.839 | (5) | | $<0.01$ | |
| 22 | 4.014 | (6) | | $<0.01$ | |
| 23 | 4.145 | (6) | | $<0.01$ | |
| 24 | 4.419 | (6) | | $<0.01$ | |
| 25 | 4.317 | (5) | | $<0.01$ | |
| 26 | 4.450 | (5) | | $<0.01$ | |
| 27 | 4.560 | (5) | | $<0.01$ | |

[a]The spectroscopic factors are from Ref. 11. The uncertainties on the excitation energy values listed in this table are of about 7 keV up to 2 MeV, 15 keV up to 3.5 MeV, and 25 keV above 3.5 MeV excitation energy in $^{117}$Sb.

## III. PROTON STRIPPING REACTIONS TO LOW-LYING STATES

### A. Data

In Figs. 1, 2, and 3 are presented the spectra from the $^{116}$Sn($\alpha$,t)$^{117}$Sb, $^{144}$Sm($\alpha$,t)$^{145}$Eu, and $^{208}$Pb($\alpha$,t)$^{209}$Bi reactions. The numbers at the top of the peaks refer to nuclear levels in $^{117}$Sb, $^{145}$Eu, and $^{209}$Bi, respectively, and the corresponding excitation energies are listed in Tables II, III, and IV, respectively.

In the case of low-lying states in $^{117}$Sb, our results are compared to those obtained in previous studies of the $^{116}$Sn($^3$He,d)$^{117}$Sb reaction.[11] The fragmentation of the valence strengths corresponding to the low-spin orbitals ($2d_{3/2}$,$2d_{5/2}$,$3s_{1/2}$) has been established, whereas very little information was available on the $1h_{11/2}$ and $1g_{7/2}$ strength distributions. Between 1.5 and 4.5 MeV excitation energy in $^{117}$Sb, the strongly excited peaks observed in the spectrum of Fig. 1 will be identified with the fragmented components of the $1h_{11/2}$ and $1g_{7/2}$ proton strengths.

For the $^{145}$Eu low-lying proton states, the high-resolution study was limited to three angles (1.75°, 3°, and 6°). Therefore only precise excitation energies have been listed in Table III up to 5.0 MeV. The quantum numbers and spectroscopic strengths for the observed states have been deduced from the thick target data analysis. The results are compared to previous proton stripping experiments.[12]

The nuclear levels of $^{209}$Bi, up to 5.7 MeV excitation energy, are listed in Table IV. Both good energy resolution and strong selectivity for large $l$ transfer ($l=5,6$) have improved our knowledge of the fragmentation of the $1h_{9/2}$, $2f_{7/2}$, $1i_{13/2}$, and $2f_{5/2}$ proton strengths in $^{209}$Bi. In addition, a number of $l=6$ and $l=7$ transitions located above 4 MeV may correspond to small components of the high-lying $1i_{11/2}$ and $1j_{15/2}$ proton subshells.

The separation of close energy levels in the spectra for valence particle states in the $^{117}$Sb, $^{145}$Eu, and $^{209}$Bi nuclei

TABLE III. Results from the analysis of the $^{144}Sm(\alpha,t)$ reaction to low-lying states.

| No. | $E_x$ (MeV) | $l$ | $J$ | $C^2S$ | $E_x$ (MeV) | $l$ | $J^\pi$ | $C^2S$ |
|---|---|---|---|---|---|---|---|---|
| | | | | | Other works[a] | | | |
| 1 | 0.000 | 2 | $\frac{5}{2}^+$ | 0.37 | 0.000 | 2 | $\frac{5}{2}^+$ | 0.33 |
| 2 | 0.327 | 4 | $\frac{7}{2}^+$ | 0.24 | 0.329 | 4 | $\frac{7}{2}^+$ | 0.17 |
| 3 | 0.711 | 5 | $\frac{11}{2}^-$ | 0.98 | 0.716 | 5 | $\frac{11}{2}^-$ | 0.82 |
| 4 | 1.043 | 2 | $\frac{3}{2}^+$ | 0.74 | 1.042 | 2 | $\frac{3}{2}^+$ | 0.98 |
| 5 | 1.610 | | | | 1.600 | 4 | $(\frac{7}{2})^+$ | 0.02 |
| 6 | 1.752 | 4 + 2 | $(\frac{7}{2})^+$ $(\frac{3}{2})^+$ | 0.13 0.15 | 1.758 | 2 | $(\frac{3}{2})^+$ | 0.02 |
| 7 | 1.856 | | | | 1.845 | 2 | $(\frac{3}{2},\frac{5}{2})^+$ | 0.10 |
| 8 | 2.113 | | | | 2.114 | 2 | $(\frac{3}{2},\frac{5}{2})^+$ | 0.04 |
| 9 | 2.215 | | | | | | | |
| 10 | 2.309 | | | | | | | |
| 11 | 2.415 | | | | | | | |
| 12 | 2.493 | | | | 2.480 | 2+0 | | 0.04+0.02 |
| 13 | 2.689 | 3 | $(\frac{7}{2})^-$ | 0.14 | | | | |
| 14 | 2.777 | | | | | | | |
| 15 | 3.237 | | | | | | | |
| 16 | 3.370 | 3 | $(\frac{7}{2})^-$ | 0.18 | | | | |
| 17 | 3.589 | | | | | | | |
| 18 | 4.364 | (5) | $(\frac{9}{2})^-$ | (0.17) | | | | |
| 19 | 4.821 | | | | | | | |
| 20 | 4.930 | | | | | | | |
| 21 | 5.149 | | | | | | | |
| 22 | 5.330 | | | | | | | |
| 23 | 5.431 | | | | | | | |

[a]Reference 12. The uncertainties on the excitation energy values listed in this table are the same as the ones mentioned in Table II.

are also necessary to obtain a measure of how well the angular distributions are described by DWBA calculations. In addition, the amount of strength exhausted in these energy regions is of importance to the discussion of the gross structure phenomena. In Sec. IV, we shall rely on these results in analyzing the data obtained for high-lying particle states.

### B. Analysis of the $(\alpha,t)$ reaction at 80 MeV

The distorted wave Born approximation (DWBA) calculations were carried out using the code DWUCK4.[15] The optical parameters employed for generating distorted waves in the entrance $(\alpha)$ channel were the fixed geometry "deep family" combination derived from the elastic scattering analysis on the $^{208}Pb$ target at 81.4 MeV incident energy.[14] For the triton exit channel, no triton elastic scattering data exist at this energy. Therefore, the triton potential selected by Perry *et al.*[14] in their study of the $^{208}Pb(\alpha,t)^{209}Bi$ reaction at 81.4 MeV was employed. This combination of parameters was found to reproduce quite well the shapes and the strengths of the first low-lying proton states in $^{209}Bi$. Standard energy separation procedure and geometry have been used to evaluate the proton form factor. These potentials are listed in Table V.

A number of low-lying transitions with known large single-particle strengths in $^{117}Sb$, $^{145}Eu$, and $^{209}Bi$, respectively, were selected to test our choice of optical parameters. The calculations were carried out in the local zero-range (LZR) approximation, without nonlocality corrections. The comparison between the experimental data and DWBA predictions are shown in Fig. 4. An excellent agreement is found between the shape of the DWBA curves and the experimental angular distributions for angular momentum transfers ranging from $l=2$ to 6. Moreover, exact finite range (EFR) calculations were performed for the same transitions using the code MARY written by Chant and Craig.[16] In the notation of Ref. 16, the range function chosen was

$$V(s)\,Y_{00}(s)=\langle \phi_b \mid V_{bx} \mid \phi_a \rangle \ ,$$

where the wave functions $\phi_i$ describing the $^3He$ and $^4He$ particles were taken as $1s$ oscillator functions with size parameters chosen to fit radii obtained from electron scattering. The ejectile nucleon interaction $V_{bx}$ was taken as a sum of singlet and triplet Gaussian nucleon-nucleon potentials which fit low energy nucleon-nucleon scatter-

TABLE IV. Results from the analysis of the $^{208}$Pb($\alpha$,t) reaction to low-lying states (0–5.7 MeV).

| No. | $E_x$ (MeV) | $l$ | $J^\pi$ | $C^2S$ | $E_x$[a] (MeV) | $l$[a] | $J^{\pi a}$ | $C^2S^{a,b}$ |
|---|---|---|---|---|---|---|---|---|
| 1 | 0.000 | 5 | $\frac{9}{2}^-$ | 0.80 | 0.000 | 5 | $\frac{9}{2}^-$ | (1–0.54) |
| 2 | 0.897 | 3 | $\frac{7}{2}^-$ | 0.76 | 0.897 | 3 | $\frac{7}{2}^-$ | (1.12–0.65) |
| 3 | 1.612 | 6 | $\frac{13}{2}^+$ | 0.74 | 1.612 | 6 | $\frac{13}{2}^+$ | (0.94–0.52) |
| 4 | 2.499 | 2 | $\frac{3}{2}^+$ | 0.014 | 2.492 | | | |
| 5 | 2.610 | 6 | $(\frac{13}{2})^+$ | 0.065 | 2.601 | 6 | $(\frac{13}{2})^+$ | (0.06–0.09) |
| 6 | 2.837 | 3 | $\frac{5}{2}^-$ | 0.57 | 2.822 | 3 | $\frac{5}{2}^-$ | (1.14–0.61) |
| 7 | 3.139 | 1 | $\frac{3}{2}^-$ | 0.44 | 3.118 | 1 | $\frac{3}{2}^-$ | (1.03–0.58) |
| 8 | 3.410 | 6 | $(\frac{13}{2})^+$ | 0.03 | 3.406 | | $(\frac{13}{2})^+$ | |
| 9 | 3.503 | 3 | $(\frac{5}{2},\frac{7}{2})^-$ | 0.04,0.03 | | | | |
| 10 | 3.650 | 1 | $(\frac{1}{2})^-$ | 0.20 | 3.633 | 1 | $(\frac{1}{2})^-$ | (0.90–0.49) |
| 11 | 3.707 | | | | | | | |
| 12 | 3.835 | 6 | $(\frac{13}{2})^+$ | 0.03 | | | | |
| 13 | 3.927 | >6 | | | | | | |
| 14 | 4.019 | >6 | | | | | | |
| 15 | 4.174 | 7 | $(\frac{15}{2})^-$ | 0.045 | | | | |
| 16 | 4.247 | 7 | $(\frac{15}{2})^-$ | 0.06 | | | | |
| 17 | 4.459 | 1 + 3 | $(\frac{1}{2})^-$ $(\frac{7}{2})^-$ | 0.10 0.10 | 4.421 4.447 | 1 3 | $(\frac{1}{2})^-$ $(\frac{7}{2})^-$ | (0.46) (0.16) |
| 18 | 4.543 | (7) | $(\frac{15}{2})^-$ | <0.02 | | | | |
| 19 | 4.613 | 3 | $(\frac{5}{2},\frac{7}{2})^-$ | 0.06,0.05 | | | | |
| 20 | 4.700 | | | | | | | |
| 21 | 4.795 | 6 | $(\frac{11}{2},\frac{13}{2})^+$ | 0.04 | | | | |
| 22 | 4.886 | 7 | $(\frac{15}{2})^-$ | 0.02 | | | | |
| 23 | 4.998 | 7 | $(\frac{15}{2})^-$ | 0.03 | | | | |
| 24 | 5.087 | 3 | $(\frac{5}{2})^-$ | 0.07 | | | | |
| 25 | 5.173 | 3 | $(\frac{5}{2})^-$ | 0.07 | | | | |
| 26 | 5.277 | 7 | $(\frac{15}{2})^-$ | 0.04 | | | | |
| 27 | 5.380 | 7 | $(\frac{15}{2})^-$ | 0.03 | | | | |
| 28 | 5.469 | 6 | $(\frac{11}{2})^+$ | 0.06 | | | | |
| 29 | 5.580 | 6 | $(\frac{11}{2})^+$ | 0.04 | | | | |
| 30 | 5.693 | (2) | $(\frac{3}{2},\frac{5}{2})^+$ | 0.15 | | | | |

[a]Reference 13.

[b]Reference 14. The errors on the excitation energy values listed in the table are of about 7 keV to 2.5 MeV, 15 keV from 2.5 to 4 MeV, and of 25 keV above 4 MeV excitation energy.

ing. We find that the LZR and EFR calculations produce nearly identical shapes, as shown in some test cases in Fig. 4. Furthermore, the ratio of cross sections EFR/LZR is state and energy independent to within about 10% for the chosen set of optical potentials. If the LZR calculations are normalized in the usual way to the volume integral $D_0$ of our chosen range function, our choice of optical model parameters leads to a EFR/LZR ratio of roughly two. This result is in agreement with the estimation of the ratio of the parameters $D^2$ and $D_0^2$ discussed by Friedman and co-workers.[17] These results are consistent with a zero-range normalization constant $N=2D^2=36$ for the ($\alpha$,t) reaction.

The deduced spectroscopic strengths for the levels used as test cases are displayed in Table II ($^{117}$Sb), Table III ($^{145}$Eu), and Table IV ($^{209}$Bi), respectively, and are in good agreement with previous determinations coming from different stripping experiments investigated at lower incident energy. Based on these various studies, in the following, our results will be compared to the LZR-DWBA calculations with the adopted normalization constant $N=36$.

### C. Results from the $^{116}$Sn($\alpha$,t)$^{117}$Sb reaction ($0<E_x<4.5$ MeV)

With the exception of the five first low-lying levels, very little spectroscopic information was available on the proton states in $^{117}$Sb. Our results are summarized in Table II. Typical angular distributions and DWBA predictions are displayed in Fig. 5.

TABLE V. Optical model potential parameters.[a]

| Channel | $V_0$ (MeV) | $r_0$ (fm) | $a_0$ (fm) | $W_0$ (MeV) | $r'_0$ (fm) | $a'_0$ (fm) | $V_{so}$ (MeV) | $r_{so}$ (fm) | $a_{so}$ (fm) | $r_c$ (fm) |
|---|---|---|---|---|---|---|---|---|---|---|
| $\alpha$ | 158.4 | 1.320 | 0.620 | 30.02 | 1.35 | 0.85 | | | | 1.4 |
| t | 125.4 | 1.18 | 0.86 | 17.20 | 1.55 | 0.77 | | | | 1.4 |
| | | | | Bound state parameters[b] | | | | | | |
| p | $V_n$ | 1.25 | 0.65 | | | | $\lambda=25$ | 1.25 | 0.65 | |

[a]Potential of the form $U(r)=-V_0 f(x)-iW_0 f(x')+V_C$, where

$$f(x_i)=\left[1+\exp\left[\frac{r-r_i A^{1/3}}{a_i}\right]\right]^{-1}$$

and $V_C$ is the Coulomb potential of a uniform sphere.

[b]Strength ($V_n$) adjusted to reproduce empirical separation energies. The binding potential is of the form

$$U(r)=-V_n\left[f(r,r_0A^{1/3},a_0)-\frac{\lambda}{45.2}\frac{1}{r}\frac{d}{dr}f(r,r_{so}A^{1/3},a_{so})L\cdot S\right],$$

where $f(r,r_iA^{1/3},a_i)$ is the Woods-Saxon form with radius and diffuseness parameters $r_{so}$ and $a_{so}$, respectively. In the case of proton states in $^{209}$Bi, a different geometry has been used with $r_0=1.28$ fm, $a_0=0.76$ fm, $r_{so}=1.09$ fm, and $a_{so}=0.60$ fm.

A large number of states with angular momentum $l=4$ and 5 are identified for the first time in this work. The strong fragmentation of the $1g_{7/2}$ and $1h_{11/2}$ proton strengths is clearly established. From the $l$ assignments and the deduced spectroscopic strengths a sum-rule analysis has been carried out. The results (centroid energy, total amount of strength) are compared in Table VI to previous determinations[18] and to the theoretical predictions of Beiner and Lombard.[19] A better determination of the $1g_{7/2}$ and $1h_{11/2}$ quasiparticle energies is obtained,

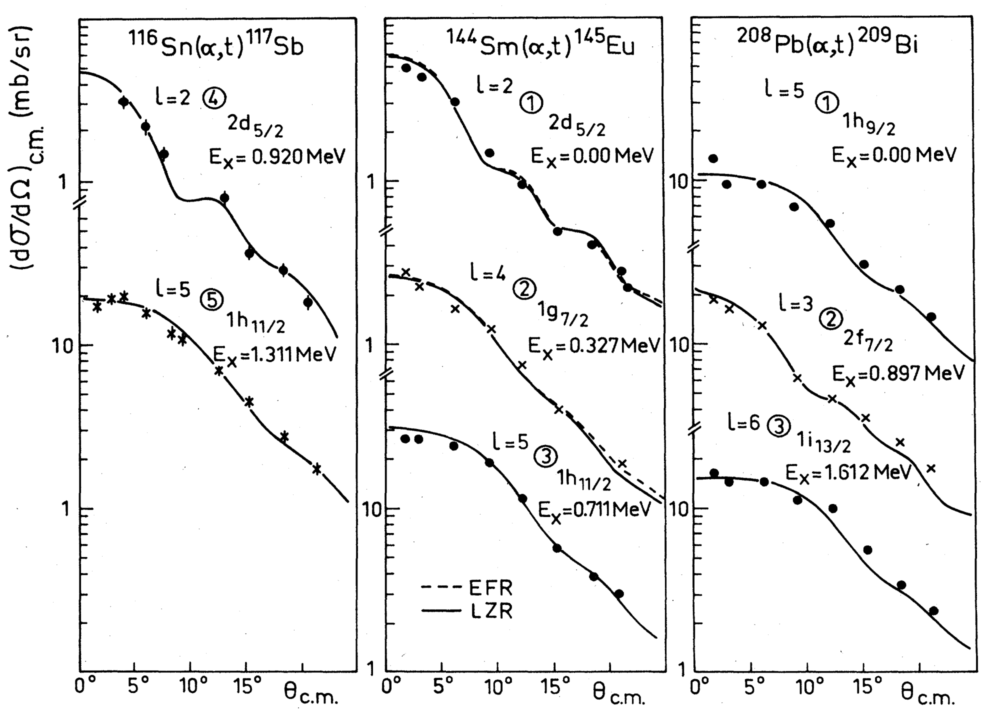


FIG. 4. Angular distributions from the $^{116}$Sn, $^{144}$Sm, and $^{208}$Pb($\alpha$,t) reactions to low-lying states in $^{117}$Sb, $^{145}$Eu, and $^{209}$Bi, respectively, with large single-particle strengths and $l$ transfers ranging from 2 to 6. The solid curves are the LZR-DWBA predictions for the indicated $l$ values. Each final state is identified by its quantum number $nlj$ and its excitation energy. The circled numbers refer to the labeling adopted for the nuclear levels in $^{117}$Sb (Table II), $^{145}$Eu (Table III), and $^{209}$Bi (Table IV). The predictions from EFR-DWBA calculations are shown as dashed lines. The optical potentials are listed in Table V. Vertical bars are statistical errors only.

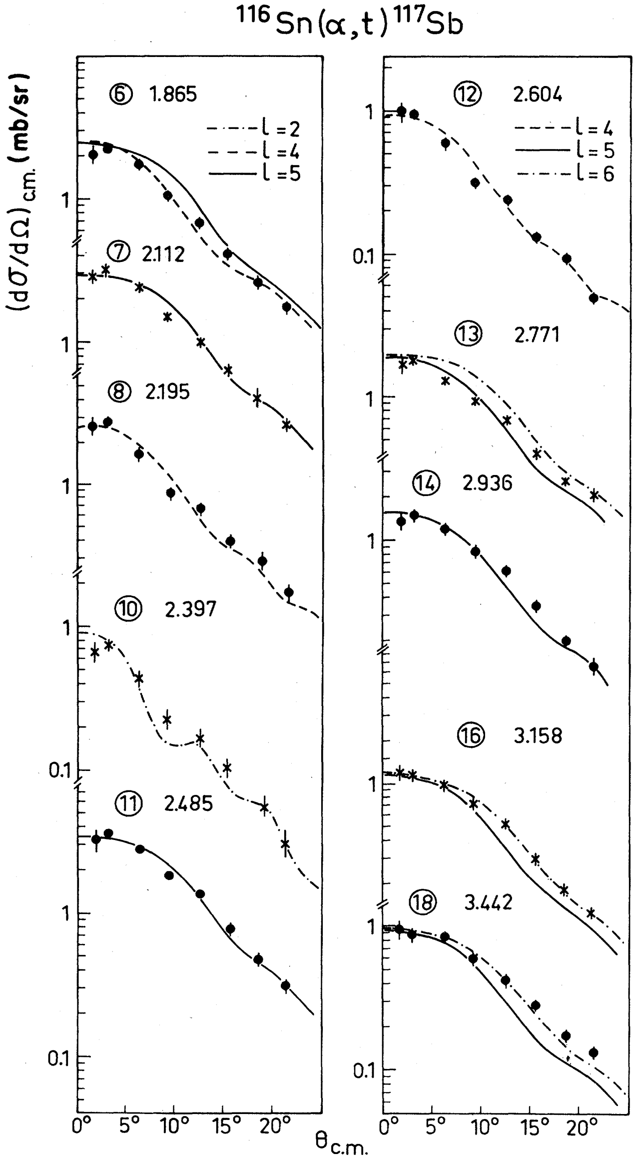


FIG. 5. Typical angular distributions from the $^{116}$Sn($\alpha$,t) reaction ($1.5 \leq E_x \leq 4.5$ MeV). The solid, dashed, and dot-dashed lines are the LZR-DWBA predictions for the indicated $l$ values. Each final state is identified by its excitation energy and number (see Table II). Vertical bars are statistical errors only.

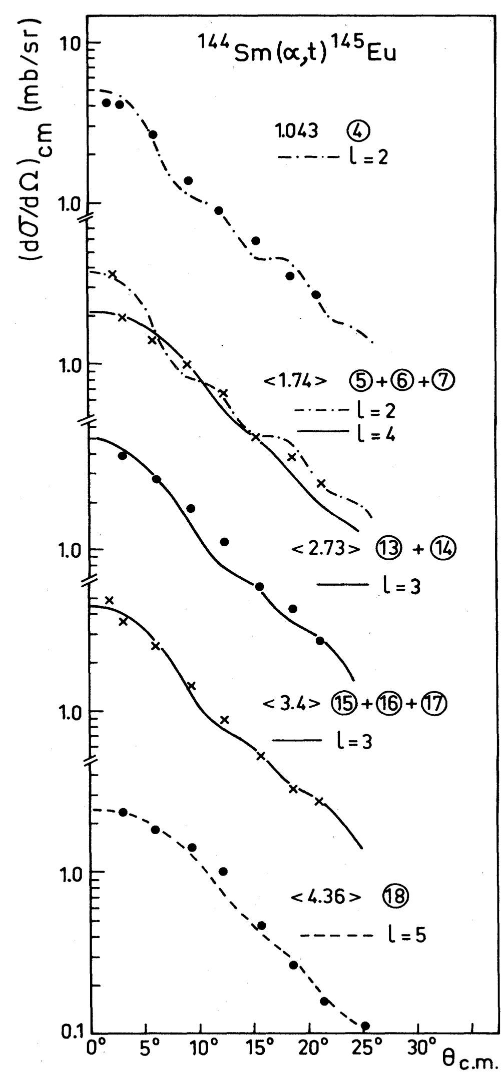


FIG. 6. Same as in Fig. 5 for the $^{144}$Sm($\alpha$,t)$^{145}$Eu reaction to low-lying states ($0 < E_x \leq 4.5$ MeV).

but the deduced values are still much lower than the predictions of Ref. 19. In addition, we would like to stress that very small components of the $l = 6$ strength are identified above 3 MeV excitation energy in $^{117}$Sb.

### D. Results from the $^{144}$Sm($\alpha$,t)$^{145}$Eu reaction ($0 < E_x < 4.5$ MeV)

The proton strength distributions of the *sdhg* shells deduced from our experiment are in close agreement with the detailed study of Wildenthal *et al.*[20] up to 2.5 MeV (see Table III). New spectroscopic information is obtained for the excitation energy of low-lying states up to 5.5 MeV in $^{145}$Eu. Significant components of the $l = 3$ strength ($2f_{7/2}$) are observed for the first time at about 2.7, 3.2, 3.4, and 3.6 MeV in $^{145}$Eu. They correspond to proton stripping to the next shell ($Z > 82$). Similarly, the well-defined peaks located between 4.0 and 5.5 MeV excitation energy are populated through an $l = 5$ transfer and may be attributed to the $1h_{9/2}$ outer subshell. In connection with the analysis of the high-lying proton excitations we will discuss this point in detail in Sec. IV. A sample of experimental angular distributions and DWBA predictions is presented in Fig. 6.

### E. Results from the $^{208}$Pb($\alpha$,t)$^{209}$Bi reaction ($0 < E_x < 5.7$ MeV)

The $^{209}$Bi nucleus has been the object of numerous proton stripping experiments due to its proton closed shell structure. The results obtained in the present

TABLE VI. Summed transition strengths $\Sigma(2j+1)C^2S$ and centroid energies $\tilde{E}_j$ for proton quasiparticle states in $^{117}$Sb $(50<Z<82)$.

| Proton subshell | $\Sigma(2j+1)C^2S$ | | | | $E_j$ (MeV) | | |
|---|---|---|---|---|---|---|---|
| | This work[a] | ($^3$He,d) 28 MeV[b] | | SRL[c] | This work | ($^3$He,d) 28 MeV[b] | $B$ and $L$[d] |
| $2d_{5/2}$ | | 5.4 | (1) | 6 | 0.00 | 0.00 | 0.00 |
| $1g_{7/2}$ | 7.92(4) | 6.6 | (4) | 8 | 1.08 | 0.81 | 0.88 |
| $3s_{1/2}$ | | 1.66 | (5) | 2 | | 1.35 | 2.55 |
| $2d_{3/2}$ | 1.72(3) | 4.57 | (6) | 4 | | 1.66 | 2.87 |
| $1h_{11/2}$ | 9.40(10) | 11 | (1) | 12 | 1.74 | 1.32 | 2.95 |

[a]The values in parentheses indicate the number of states belonging to the $nlj$ subshells observed in the present study. The numbers have the same meaning in the case of the ($^3$He,d) study at 28 MeV.
[b]Reference 18. The data were reanalyzed assuming that all the $l=2$ states except the ground state belong to the $2d_{3/2}$ subshell.
[c]Sum-rule limit $S=(2j+1)p_j-[(2T_0+1)]^{-1}n_j$; $p_j$ and $n_j$ are the proton and neutron occupation probabilities of the $nlj$ subshells in the target ground state. Due to the shell closure at $Z=50$, $p_j=1$, and here $2T_0=16$, $n_j$ is always smaller than 1. Therefore $(2T_0+1)^{-1}\times n_j \ll 1$, and the sum rule limit is equal to $(2j+1)$.
[d]Reference 19.

$^{208}$Pb($\alpha$,t)$^{209}$Bi study are summarized in Table IV. Below 5.7 MeV excitation energy about 30 levels are observed. Definite $l$ values and spectroscopic factors have been assigned to practically all the excited states due to the good resolution and good statistics. Some typical angular distributions from the ($\alpha$,t) study are displayed in Fig. 7.

As compared to previous proton stripping studies,[13] our results are in good agreement with the existing data on proton particle-state fragmentation in $^{209}$Bi up to 3.7 MeV excitation energy (see Table IV). However, we would like to point out that the deduced spectroscopic strengths were obtained using a slightly different geometry for the proton form factor (see Table V) close to the values of the Woods-Saxon potential parameters of Brown *et al.*[21] ($r_p=1.27$ fm, $a_p=0.81$ fm, $r_{so}=1.1$ fm, and $a_{so}=0.65$ fm). This set of parameters was found to reproduce nicely the single-particle energies near the Fermi surface, the radius, and the diffuseness of the density in $^{208}$Pb. The usual geometry parameters ($r_p=1.25$ fm, $a_p=0.65$ fm) give unrealistic results, exceeding by a large amount (50–80%) the sum rule for the first low-lying $1h_{9/2}$, $2f_{7/2}$, and $1i_{13/2}$ single-particle states.

The detailed analysis carried out up to 5.7 MeV in $^{209}$Bi leads to the observation of a number of new features with

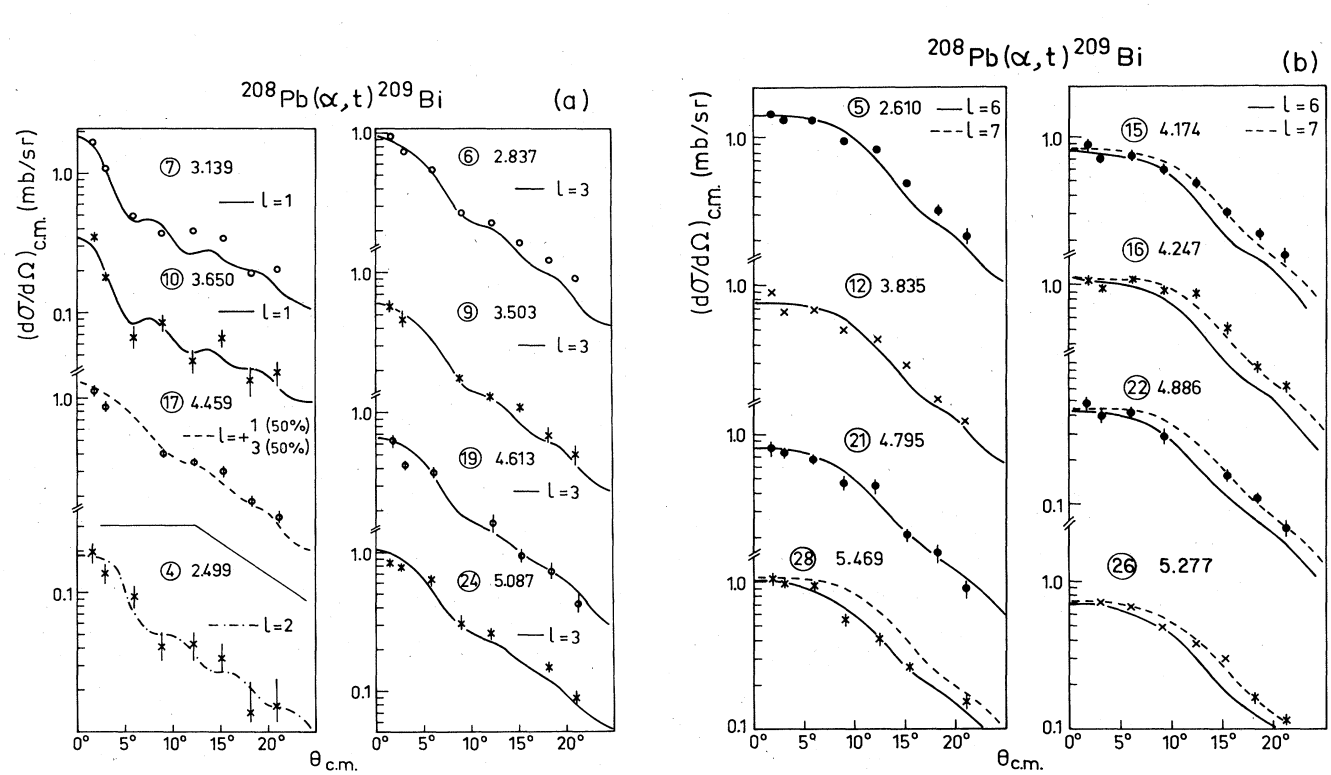


FIG. 7. Same as in Figs. 4–6 for the $^{208}$Pb($\alpha$,t)$^{209}$Bi reaction to low-lying states ($0\leq E_x\leq 5.7$ MeV).

TABLE VII. Summed transition strengths and centroid energies of proton states in $^{209}$Bi belonging to the *hfip* shell.

| *nlj* | $\Sigma C^2S$[a] | $\tilde{E}_j$ | $\tilde{E}_j$[b] | $E_j$[c] | $E_j$[d] |
|---|---|---|---|---|---|
| $1h_{9/2}$ | 0.80(1) | 0.000 | 0.00 | 0.00 | 0.00 |
| $2f_{7/2}$ | 0.86(2) | 1.310 | 1.50 | 0.81 | 1.72 |
| $1i_{13/2}$ | 0.90(5) | 1.970 | 1.71 | 1.75 | 1.90 |
| $3p_{3/2}$ | 0.44(1) | (3.14) | 3.12 | 4.12 | 5.67 |
| $3p_{1/2}$ | 0.30(2) | (3.91) | 3.97 | 5.32 | 6.10 |
| $2f_{5/2}$ | 0.81(5) | 3.44 | 2.82 | 3.70 | 4.27 |

[a]The values quoted in parentheses indicate the numbers of states belonging to the *nlj* subshell.
[b]Reference 21 (deduced values based on data from Ref. 13).
[c]Theoretical predictions of quasiparticle energies from Beiner and Lombard (Ref. 19).
[d]Centroid energies of proton states in $^{209}$Bi from Ref. 22.

regards to the fragmentation of the $1i_{13/2}$ and $2f_{5/2}$ subshells. A number of new $l=6$ transitions are evidenced in this work. New $l=3$ components are observed around 5 MeV in $^{209}$Bi. But the most important result is the observation of seven states populated through an $l=7$ transfer and therefore arising from the fragmentation of the high-spin outer $1j_{15/2}$ proton subshell. For the proton states belonging to the *hfip* shell ($82<Z<126$), a sum-rule analysis has been carried out and the deduced centroid energies and summed transitions strengths are listed in Table VII.

More than 80% of the sum rule is found for the $1h_{9/2}$, $2f_{7/2}$, $1i_{13/2}$, and $2f_{5/2}$ proton orbitals. The deduced centroid energies are in good agreement with previous determinations[21] and with the predictions from various microscopic theories.[19,22] Since a larger fragmentation of the

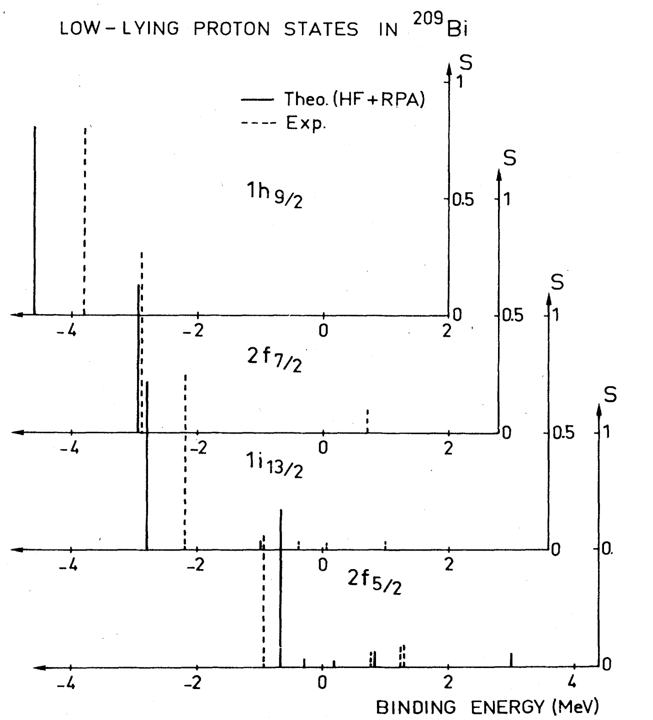


FIG. 8. Comparison between experimental and theoretical (Ref. 22) proton strengths for the low-lying $1h_{9/2}$, $2f_{7/2}$, $1i_{13/2}$, and $2f_{5/2}$ subshells in $^{209}$Bi.

$2f_{5/2}$ and $1i_{13/2}$ proton subshells is observed in this work, the resulting centroid energies are closer to the theoretical values. The results obtained here for the $3p_{3/2}$ and $3p_{1/2}$ proton strengths are very limited and no meaningful comparison can be made with previous results or theoretical predictions (see Table VII).

In Fig. 8, the fragmentation of the $1h_{9/2}$, $2f_{7/2}$, $1i_{13/2}$, and $2f_{5/2}$ proton subshells is compared to the theoretical calculations of Van Giai and Van Thieu.[22] A self-consistent microscopic approach is used to calculate the proton single-particle spectrum in $^{209}$Bi. The Hartree-Fock field with Skryrme force is used to generate the single-particle states and the random-phase approximation (RPA) method to calculate the collective excitations of the core. Then coupling between single-particle and vibration states is achieved in order to reproduce the fragmentation of the single-particle strengths. The observed agreement between theory and experiment both for the binding energies and the strengths is quite good, especially if one recalls that there are no free parameters in the microscopic calculation of Van Giai and Van Thieu.[22]

## IV. HIGH-LYING PROTON STRENGTH DISTRIBUTIONS

### A. Data

An important step has recently been made towards the use of the one nucleon transfer reactions for the study of high-lying nuclear excitations.[8] A new type of "resonancelike structure" has been observed in the study of the proton stripping reaction ($\alpha$,t) on a number of medium-heavy target nuclei ($^{116}$Sn, $^{114}$Sm, and $^{208}$Pb).

The general behavior of the particle response function, up to high excitation energy (22 MeV), is illustrated in Fig. 9. Above the energy range which has been discussed in Sec. III (valence proton strengths), gross structure peaks ($A$ and $B$) are clearly observed in the three spectra of Fig. 9 between 5 and 15 MeV.

The high energy part (15—25 MeV) of the three spectra does not exhibit pronounced structures and has quite similar shapes. It has been shown by Wu *et al.*[23] and by Budzanowski *et al.*[24] that the breakup processes give an important contribution to the reaction cross section of fast alpha particles scattered on medium-heavy weight nuclei. An attempt to describe the underlying continuum using a

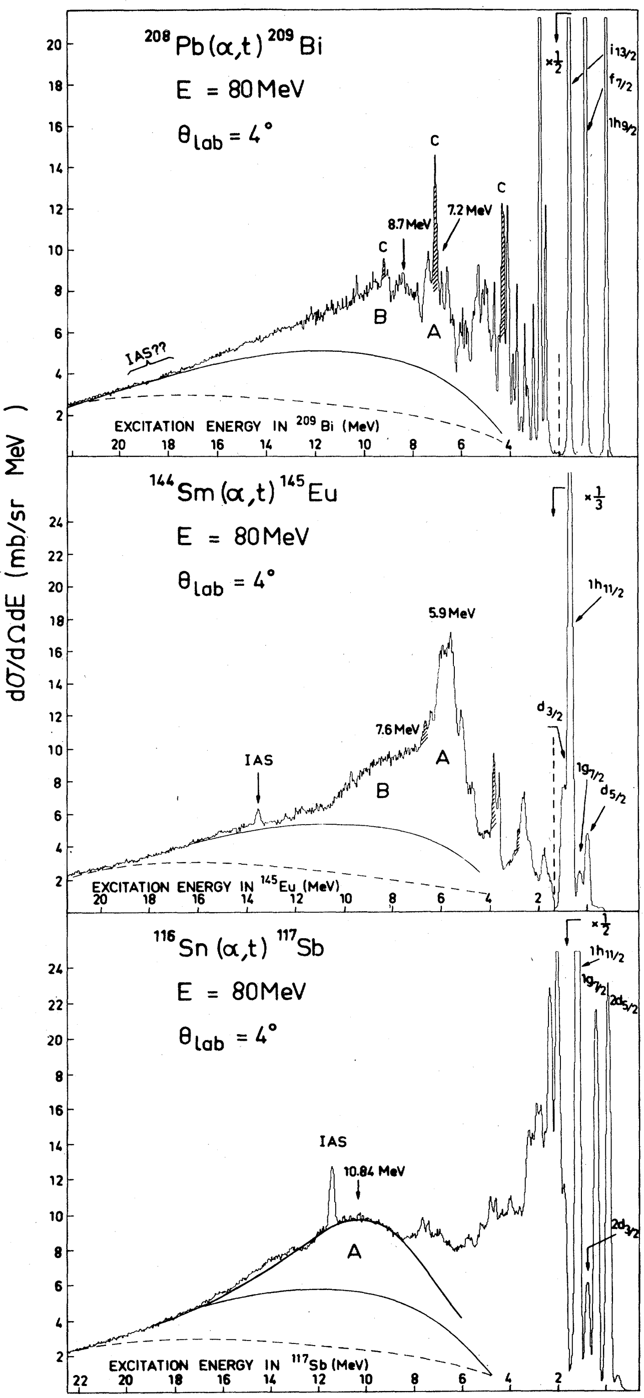


FIG. 9. Residual energy spectra from the (α,t) reaction on $^{116}$Sn, $^{144}$Sm, and $^{208}$Pb targets. The vertical scale indicates the double differential cross sections in mb/sr per MeV. On the horizontal scales are plotted the excitation energies. The solid lines are the empirical background line shapes. The dashed curves are the predictions of the PWBU model (see the text). The hatched areas refer to the positions of the contaminant peaks. The regions where a large concentration of high-lying proton strengths is observed are labeled $A$ and $B$.

simple Serber plane wave breakup model[25] (PWBU) will be described in Sec. IV B.

Around 11.5 MeV in $^{117}$Sb and 14 MeV in $^{145}$Eu, sharp peaks ($\Gamma < 200$ keV) are also populated. Simple Coulomb displacement energy calculations predict that the $T_>$ part of high-lying proton strengths or the isobaric analog states should be located at these excitation energies in $^{117}$Sb and $^{145}$Eu, respectively. We would like to stress that the IAS in $^{209}$Bi expected between 18 and 20 MeV are not observed above the underlying continuum (see Fig. 9). The amount of proton strength located in the IAS is proportional to $1/2T_>$, where $T_>$ is the isospin of the analog configuration. For IAS in $^{209}$Bi, $T_> = \frac{45}{2}$, therefore the very small amount of strength ($\sim 2\%$ of the sum rule) and the large continuum cross section ($\sim 3$ mb/sr MeV) may explain that such excitations are not seen in the present study.

### B. Background line shape and breakup calculations

The extraction of the differential cross sections for the gross structure peaks $A$ and $B$ (see Fig. 9) implies an assumption on the background line shape. The weak dependence of the background yield versus the atomic number $A$ of the target observed in this study reinforces our interpretation, namely that the main part of the cross section found in the underlying continuum comes from the breakup of the $\alpha$ particle. Plane-wave breakup calculations including corrections due to the Coulomb force were carried out in order to have an estimate of the elastic breakup contribution to the continuum cross sections. The method developed by Matsuoka *et al.*[26] was employed. The theoretical predictions were normalized to the data at forward angles ($\theta < 6°$) and at high excitation energy ($E_x \simeq 22$ MeV). The results are shown as dashed lines in Fig. 9. A close examination of the residual energy spectra indicates that a substantial amount of cross section located between 5 and 20 MeV excitation energy cannot be explained by the elastic breakup. Moreover, our estimate of the "background" cross sections does not take into account the inelastic breakup process where a subset of the projectile (here the t particle) interacts strongly with the target while the remaining fragment acts as a spectator. No further attempt was made to unravel the cross section observed in that energy range in an inelastic breakup and a stripping component.

The failure of this simple PWBU model in the case of the (α,t) reaction leads us to use the so-called "empirical background line shape." In Fig. 9, the solid lines, which smoothly connect the structureless part of the spectra to the minima of cross sections near 4 to 6 MeV, represent that assumption. We would like to stress that the adopted background line has to be considered as an upper estimate since part of the stripping cross sections to high-lying proton states may be contained in the substracted background.

### C. Analysis: Strength distributions and comparison to nuclear models

#### 1. *High-spin outer subshells in $^{117}$Sb*

The detailed analysis of the low-lying proton states in $^{117}$Sb has shown that most of the strength belonging to the

TABLE VIII. Characteristics of high-lying proton states in $^{117}$Sb. $T_0$ is the isospin of the target ground state ($^{116}$Sn, $T_0=8$).

| Bump | $E$ (MeV) | $E_{qp}$ ($1h_{9/2}$) | $E_{qp}$ ($1i_{13/2}$) | $\Gamma$ (MeV) | $nlj$ | $C^2S$ |
|---|---|---|---|---|---|---|
| $A$ | $10.84\pm0.3$ | 11.52[a] | 11.45[a] | $5.5\pm0.6$ | $1h_{9/2}$ | 1.09 |
| | | | 12.25[b] | | $1i_{13/2}$ | 0.28 |
| IAS | $E_x$ (MeV) | $E_x$ (parent)[c] | $l$ $J^\pi$ | $C^2S$ (parent)[c] | $(2T_0+1)C^2S$ | |
| | $11.59\pm0.05$ | 0.314 | 5 $\frac{11}{2}^-$ | 0.79—0.62 | 0.53 | |

[a]Reference 19.
[b]Reference 27.
[c]Reference 11.

*sdhg* shell is exhausted below 4.5 MeV (see Sec. III C and Table VI). The broad enhancement of cross section observed in Fig. 9 between 7 and 17 MeV excitation energy may arise from proton stripping to outer subshells ($2f_{7/2}$, $1h_{9/2}$, and $1i_{13/2}$). The yield in the energy range of interest has been extracted after substraction of a "smooth" background as indicated by the horizontal solid line in Fig. 9. The gross structure ($A$ in Fig. 9) has been fitted by a Gaussian, the characteristics of which (centroid energy, width) are listed in Table VIII.

The deduced angular distribution for the bump $\langle A \rangle$ located around 10.84 MeV in $^{117}$Sb is presented in Fig. 10 together with the one of the IAS at 11.59 MeV. Since these excitations lie above the proton threshold ($S_p=4.41$ MeV), the DWBA calculations have been made using resonant form factors[28] to describe the unbound proton.

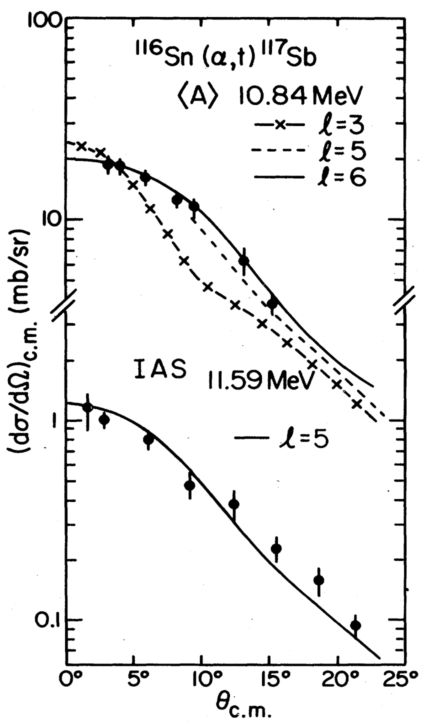


FIG. 10. Angular distributions for the gross structure $A$ and for the IAS from the $^{116}$Sn($\alpha$,t) reaction. The solid, dashed, and dot-dashed curves are the LZR-DWBA predictions for the indicated $l$ values. Vertical bars are statistical errors only. The unbound state form factor has been calculated using the resonance method (see the text).

For the gross structure $A$, the data is rather well produced by an $l=5$ ($1h_{9/2}$) or an $l=6$ ($1i_{13/2}$) transfer whereas the $l=3$ assumption does not agree with the experimental angular distribution (see Fig. 10). The amount of high-lying proton strength located in the bump $A$ is equal to 28% of the sum-rule limit if one assumes a proton stripping to the $1i_{13/2}$ outer subshell or to 100% in the case of the $1h_{9/2}$ orbital (see Table VIII). From our data and the resulting analysis it is not possible to unravel the two components of the strength distributions. Moreover, the theoretical predictions[19,27] indicate a strong overlap of the $1h_{9/2}$ and $1i_{13/2}$ proton strengths in $^{117}$Sb.

With regards to the sharp state observed at 11.59 MeV, its excitation energy and angular distribution (see Fig. 10) agree with its identification as the IAS of the $E_x=0.314$ MeV, $J^\pi=\frac{11}{2}^-$ state in $^{117}$Sn. This level has been previously observed in a study of the $^{116}$Sn($^3$He,d) reaction by Strohbusch *et al.*,[29] but no analysis has been attempted. The DWBA calculation was carried out assuming a $1h_{11/2}$ proton resonance ($E_p=7.18$ MeV) and the deduced transition strength is in reasonable agreement with the one of the parent state (see Table VIII).

### 2. *The $2f_{7/2}$, $1h_{9/2}$, and $1i_{13/2}$ proton strength distributions in $^{145}$Eu*

The first results of the high-lying proton strength distributions in $^{145}$Eu have been reported previously.[8] In this section, a summary of the analysis will be given, along with a comparison of the deduced strength distributions with the predictions for the quasiparticle-phonon coupling nuclear model.[27] The $^{145}$Eu energy spectrum for the ($\alpha$,t) reaction is presented in Fig. 9. At high excitation energy ($E_x>4$ MeV), two broad bumps are strongly excited above a substantial background. Around 14 MeV, a sharp peak corresponding to the $1h_{9/2}$ and/or to the $1i_{13/2}$ IAS is observed for the first time. The characteristics of the gross structure peaks ($A$ and $B$) were extracted assuming an empirical background line shape (solid line, Fig. 9). The remaining part of the cross section was fitted by two Gaussian peaks having different widths. The result of this fitting procedure is presented in Fig. 11(a). A DWBA analysis of the high-lying peaks $A$ and $B$ was carried out taking into account the unbound nature of the transferred proton.[8] It was found that the full $l=5$, $1h_{9/2}$ proton strength lies in the bump $A$ with a possible 20% admixture of $l=3$, $2f_{7/2}$ strength and that the $l=6$ $1i_{13/2}$ pro-

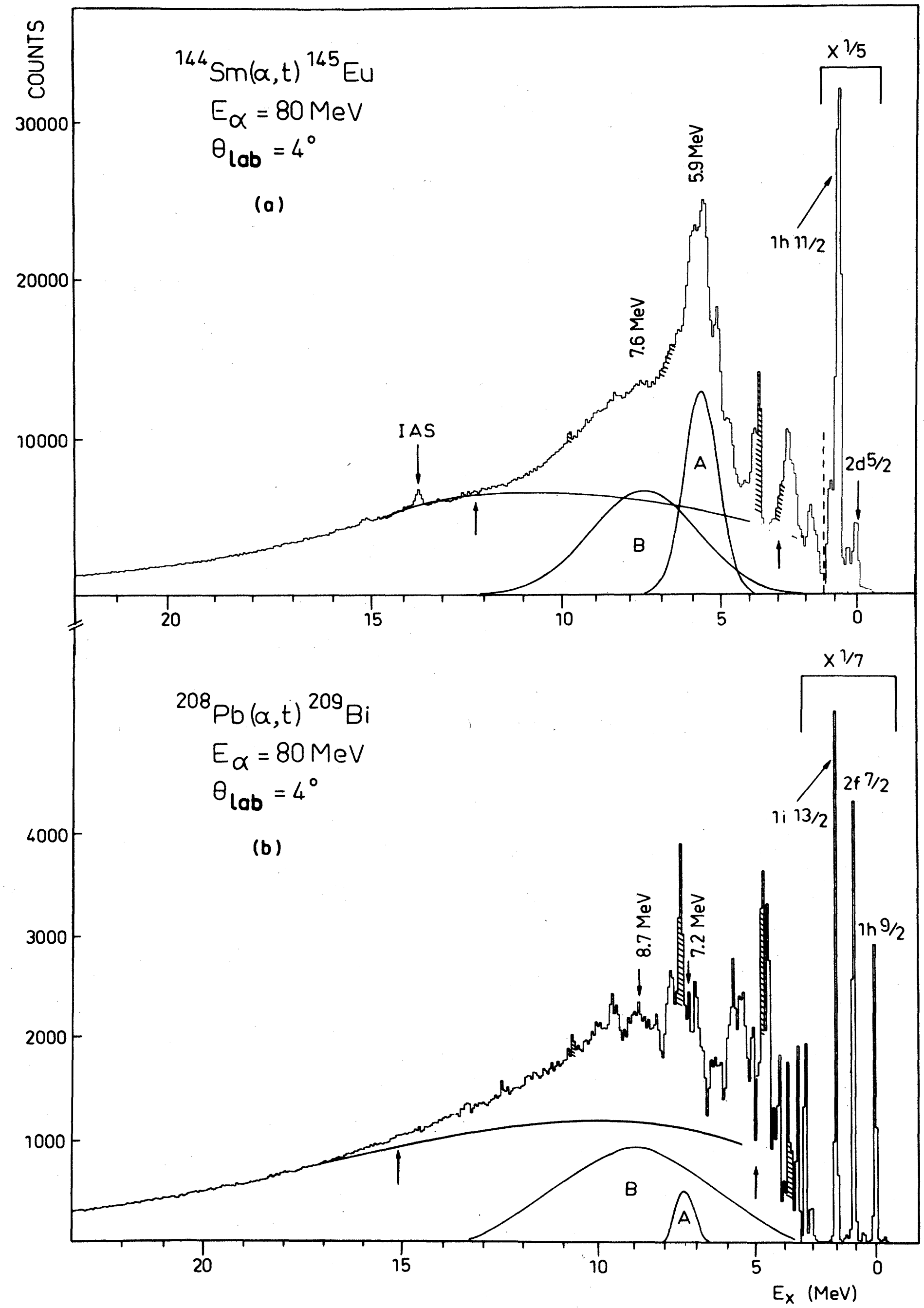


FIG. 11. (a) Triton energy spectrum from the reaction $^{144}$Sm$(\alpha,t)^{145}$Eu at a laboratory angle of 4°. The solid horizontal line indicates the shape of the empirical background. The hatched areas refer to the position of the contaminant peaks. The gross-structure peaks $A$ and $B$ are fitted by two Gaussian curves. The vertical arrows show the limits of the energy range considered for the analysis of the high-lying proton states. (b) Same as (a) for the reaction $^{208}$Pb$(\alpha,t)^{209}$Bi.

ton strength is concentrated in region $B$ (see Table I, Ref. 8).

In order to have a meaningful comparison with the strength function calculated within the quasiparticle-phonon coupling nuclear model, the energy range between 3 and 12 MeV excitation energy in $^{145}$Eu was divided into adjacent bins 1 MeV wide. The resulting differential cross sections (after subtraction of the background) were compared to the DWBA predictions assuming $l=3$, 5, or 6 transfers.

Typical experimental angular distributions and DWBA curves are shown in Fig. 12. The lower energy bins are better reproduced by an $l=5$ transfer, whereas the angular distributions of the higher energy part are best fitted

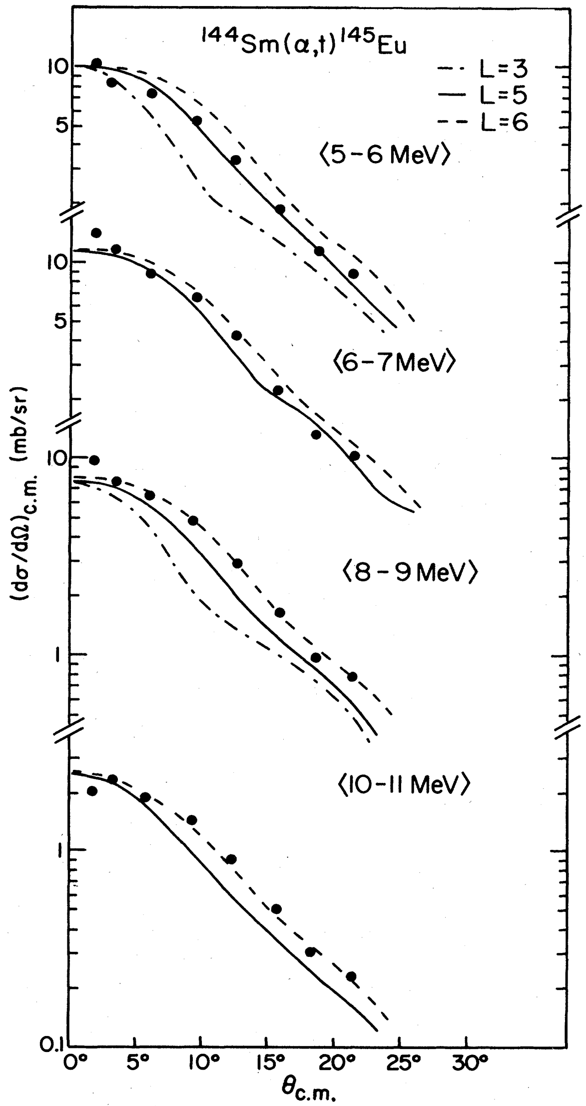


FIG. 12. Typical angular distributions and DWBA curves from the reaction $^{144}$Sm$(\alpha,t)^{145}$Eu to high-lying proton states. The solid, dashed, and dot-dashed curves are the LZR-DWBA predictions for the indicated $l$ values.

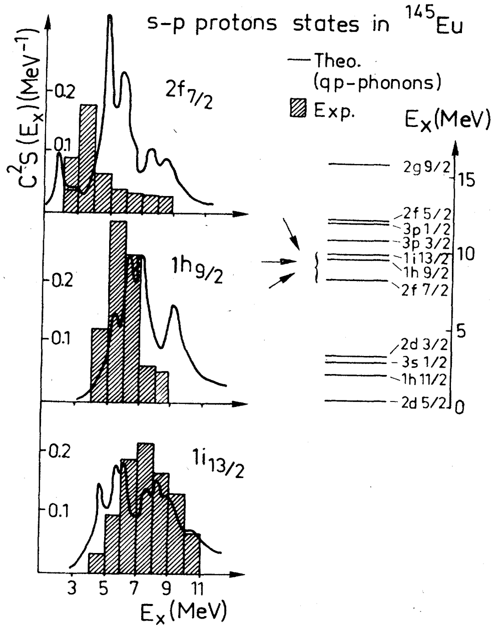


FIG. 13. Comparison between theoretical (Ref. 27) and experimental proton strength distributions for high-lying subshells in $^{145}$Eu. On the right-hand side of the figure is displayed the level scheme of proton quasiparticle states calculated in a Woods-Saxon potential (Ref. 27).

by an $l=6$ transfer. These conclusions are in good agreement with the previous analysis where Gaussian shapes were used to deduce the angular dependence of the high-lying states.[8]

In Table IX are summarized the properties of the high-lying states in $^{145}$Eu. The results (energy range, centroid energies, widths, fraction of the sum rule) are compared to the predictions from the quasiparticle phonon model.[27] In Fig. 13 are presented the experimental and theoretical strength functions (unit of strength per unit energy interval) for the $2f_{7/2}$, $1h_{9/2}$, and $1i_{13/2}$ outer subshells in $^{145}$Eu. The agreement with the experiment is quite good for the $1i_{13/2}$ subshell, whereas the empirical centroid energies of the $2f_{7/2}$ and $1h_{9/2}$ strength distributions disagree by 1 to 2 MeV with the predictions of Stoyanov and Vdovin.[27] Moreover, the damping of the $1h_{9/2}$ strength is rather large compared to the experimental one (see Table IX and Fig. 13). For the $2f_{7/2}$ and $1h_{9/2}$ subshell such disagreement may be partly explained by a less accurate determination of the experimental strengths in the overlapping regions.

The empirical spin-orbit splitting for the $1h_{9/2}$-$1h_{11/2}$ subshells is found equal to 5.2 MeV, whereas the theoretical calculations of Beiner and Lombard[19] and of the Dubna group[27] predict a value of 7.2 and 7.4 MeV, respectively. The $T_>$ part of these high-lying proton states is observed at 13.74 MeV excitation energy in $^{145}$Eu. The deduced angular distribution is displayed in Fig. 14 and compared to DWBA predictions for an $l=5$ ($1h_{9/2}$) and an $l=6$ ($1i_{13/2}$) proton resonance. A reasonable agreement with the data is observed for both assumptions. The deduced spectroscopic strengths are compared in Table IX to the ones of the $E_x=1.099$ MeV, $J^\pi=\frac{13}{2}^+$ and $E_x=1.430$, $J^\pi=\frac{9}{2}^-$ states in $^{145}$Sm. The excitation energy and the angular distribution of the 13.74 MeV state in $^{145}$Eu are considered as strong arguments in favor of its identification as the IAS of the $E_x=1.099$ MeV, $J^\pi=\frac{13}{2}^+$ state in $^{145}$Sm.

### 3. *The high-spin outer subshells in $^{209}$Bi*

The analysis of the low-lying and discrete peaks in $^{209}$Bi has shown that most of the proton strength belonging to the *hfpi* shell ($82<Z<126$) is exhausted below 5 MeV (see Sec. III E and Table VII). Small components of the $l=7$ ($1j_{15/2}$) and $l=6$ ($1i_{11/2}$) strengths are excited be-

TABLE IX. Characteristics of high-lying proton states in $^{145}$Eu. Comparison with the predictions of the quasiparticle-phonon coupling nuclear model.

| $nlj$ | | $E_i - E_f$ (MeV) | $\tilde{E}$ (MeV) | $\Gamma$ (MeV) | $\Sigma C^2 S$ (%) | |
|---|---|---|---|---|---|---|
| $2f_{7/2}$ | expt | 2–9 | 4.3±0.5 | 1.8±0.4 | 43 | |
| | theo[a] | 0–12 | 5.64 | 2.26 | 86 | |
| $1h_{9/2}$ | expt | 3–12 | 5.92±0.1 | 1.23±0.15* | 75 | |
| | theo[a] | 0–14 | 7.83 | 4.77 | 51 | |
| $1i_{13/2}$ | expt | 3–12 | 7.63±0.4 | 4.00±0.5* | 54 | |
| | theo[a] | 0–14 | 7.81 | 5.3 | 88 | |
| | $E_x$ (MeV) | $E_x - E_0$ (MeV)[b] | $E_x$ (parent state) (MeV)[b] | $nlj$ | $Sdp$[b] | $S_>$[c] |
| IAS | | | | | | |
| | 13.74±0.04 | 1.17±0.05 | 1.099 | $1i_{13/2}$ | 0.46 | 0.24 |
| | | | 1.430 | $1h_{9/2}$ | 0.64 | (0.83) |

[a]Reference 27. * is deduced from the Gaussian shapes [see Fig. 11(a)].
[b]$E_x$ is the excitation energy of the ground state analog in $^{145}$Eu. The excitation energies, quantum numbers, and spectroscopic strengths of the parent states in $^{145}$Eu are from Ref. 12.
[c]$S_> = (2T_0+1)C^2S$, $T_0$ is the isospin of the $^{144}$Sm ground state and $C^2S$ the spectroscopic strength extracted from the IAS angular distribution.

tween 4 and 6 MeV excitation energy.

The residual energy spectrum for the $^{208}$Pb($\alpha$,t)$^{209}$Bi reaction is displayed in Fig. 11(b). Above the region of discrete peaks, broad enhancement of cross sections extending up to 15 MeV dominate the high-energy part of the $^{209}$Bi energy spectrum. The solid line which smoothly connects the structureless part of the spectrum to the minima of cross sections near 6.5 and 4.5 MeV has been adopted as an empirical background lineshape. The remaining part of the cross section was extracted in two different ways.

(i) A fit using two Gaussian peaks with different widths ($A$ and $B$) reproduces nicely the energy spectrum at all angles. The result of this procedure is shown in Fig. 11(b). The deduced centroid energies and widths are listed in Table X.

(ii) The energy range of interest (5 to 15 MeV) was divided into adjacent bins, 1 MeV wide.

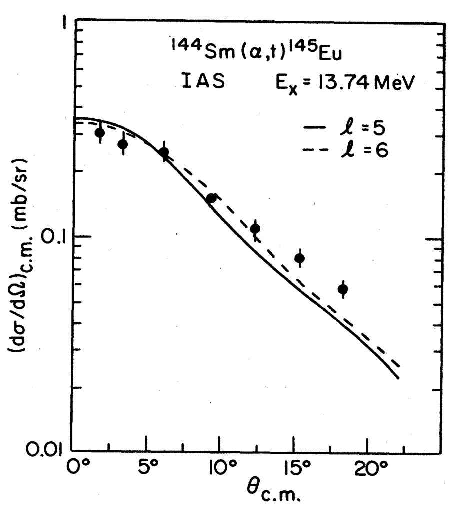


FIG. 14. Experimental angular distribution for the 13.74 MeV IAS in $^{145}$Eu from the $^{144}$Sm($\alpha$,t)$^{145}$Eu reaction. The solid and dashed curves are the LZR-DWBA predictions for the indicated $l$ values. The unbound proton form factor has been calculated using the resonance method (see the text). Vertical bars are statistical errors only.

The experimental data and DWBA curves for the bumps $A$ and $B$, and for some typical energy bins (6–7, 8–9, 11–12 MeV), are shown in Fig. 15. The deduced angular distributions using the two methods give consistent results. A better fit is obtained between 5 and 7 MeV if one assumes an $l=6$ transfer, whereas the high energy part is well reproduced by an $l=6$ and/or an $l=7$ transfer. We would like to point out that the $l=4$ DWBA curves do not agree with the empirical data (see Fig. 15), although from shell model predictions the first high-spin outer subshells to be considered are the $1j_{15/2}$ ($l=7$), $2g_{9/2}$ ($l=4$), and $1i_{11/2}$ ($l=6$). The angular distribution at high excitation energy ($E_x \sim 20$ MeV) is shown in Fig. 15. The slope of the data is much less steep than the ones obtained in the gross structure regions. The background angular distribution agrees nicely with the prediction of the PWBU model as displayed in Fig. 15. A similar analysis has been carried out for the background in the case of the reactions $^{116}$Sn($\alpha$,t)$^{117}$Sb and $^{144}$Sm($\alpha$,t)$^{145}$Eu. The deduced results are identical, both in magnitude (3–4 mb/sr MeV) and overall trend to the one obtained here from the $^{208}$Pb($\alpha$,t) reaction. This result reinforces our assumption that the cross section at

TABLE X. Characteristics of high-lying proton strengths in $^{209}$Bi. Comparison with the predictions from the quasiparticle-phonon and single particle-vibration coupling nuclear models.

| Bumps | | $\widetilde{E}$ (MeV) | $\Gamma$ (MeV) | $l$ | $\Sigma C^2S$ (%) |
|---|---|---|---|---|---|
| $A$ | | 7.2±0.2 | 0.63±0.2 | 6 + 7 | 6<br>2 |
| $B$ | | 8.7±0.5 | 5.3±1.0 | 6 + 7 | 57<br>57 |
| **Energy bins** | | $E_i - E_f$ (MeV) | $\widetilde{E}$ (MeV) | $\Gamma$ (MeV) | $\Sigma C^2S$ (%) |
| $1i_{11/2}$ | expt | 4—13 | 7.80 | 4.8 | 72 |
| | theo[a] | 0—12.5 | 8.37 | 4.9 | 90 |
| | theo[b] | 0—13 | 9.20 | | 80 |
| $1j_{15/2}$ | expt | 4—13 | 7.40 | 5.4 | 77 |
| | theo[a] | 0—12.5 | 7.10 | 5.5 | 86 |
| | theo[b] | 0—13 | 9.50 | | 81 |

[a]Reference 27.
[b]Reference 22.

very high excitation energy ($E_x > 20$ MeV) arises from the breakup of the $\alpha$ particles.

The proton strength distributions are compared in Figs. 16(a) and (b) to the theoretical predictions from the quasiparticle phonon[27] [Fig. 16(a)] and the single-particle vibration[22] [Fig. 16(b)] coupling nuclear models. The experimental strengths were extracted from the DWBA analysis of the discrete peaks (4 to 5 MeV) and of the energy bins (6 to 13 MeV). In the latter case, since $l=6$ and 7 transfers reproduce the data equally well (see Fig. 15), we have assumed an equal weight for the $l=6$ and 7 components.

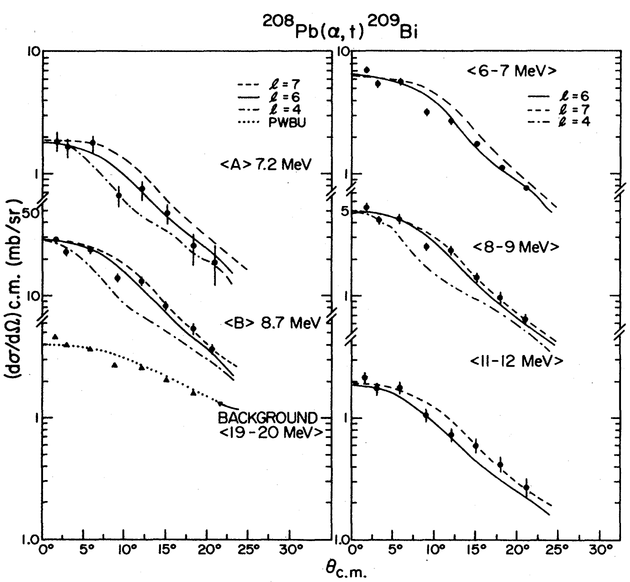


FIG. 15. Experimental angular distributions and DWBA curves from the reaction $^{208}$Pb($\alpha$,t)$^{209}$Bi to high-lying proton states. The solid, dashed, and dot-dashed curves are LZR-DWBA predictions for the indicated $l$ values. The energy bin or the centroid energy of interest is displayed. The dotted curve corresponds to the prediction of the PWBU model (see the text).

The characteristics of the high-lying proton strengths are compared to the corresponding quantities from the theoretical models in Table X. The first two moments of the empirical distributions (centroid energies and widths) are in a reasonable agreement with the expectations from the quasiparticle-phonon coupling scheme. More than 70% of the $l=6$ $1i_{11/2}$ and of the $l=7$ $1j_{15/2}$ proton strength is found in the energy range 4—13 MeV in $^{209}$Bi in agreement with the theoretical predictions. However, the details of the strength functions are not well reproduced by the model where specific peaks predicted at 7.5 and 9.5 MeV for the $1i_{11/2}$ distribution and at 7 MeV for the $1j_{15/2}$ case are not observed experimentally.

With regard to the comparison with the predictions from the single-particle vibrations model of Van Giai and Van Thieu,[22] the centroid energies and the structure of the response functions do not agree with the empirical data [see Fig. 16(b)]. It appears that the predicted damping of the single-particle strengths is smaller at least by a factor of 2 as compared to the experiment. Only the total amount of $1i_{11/2}$ and $1j_{15/2}$ proton strength located between 4 and 13 MeV is very close to the experimental values (see Table X).

In addition, this analysis allows us to extract the strength of the spin-orbit potential for the $1i_{13/2}$-$1i_{11/2}$ orbitals. The experimental value is equal to 5.83 MeV, whereas the various theoretical expectations lie between 7.1 and 7.6 MeV.[19,22,27]

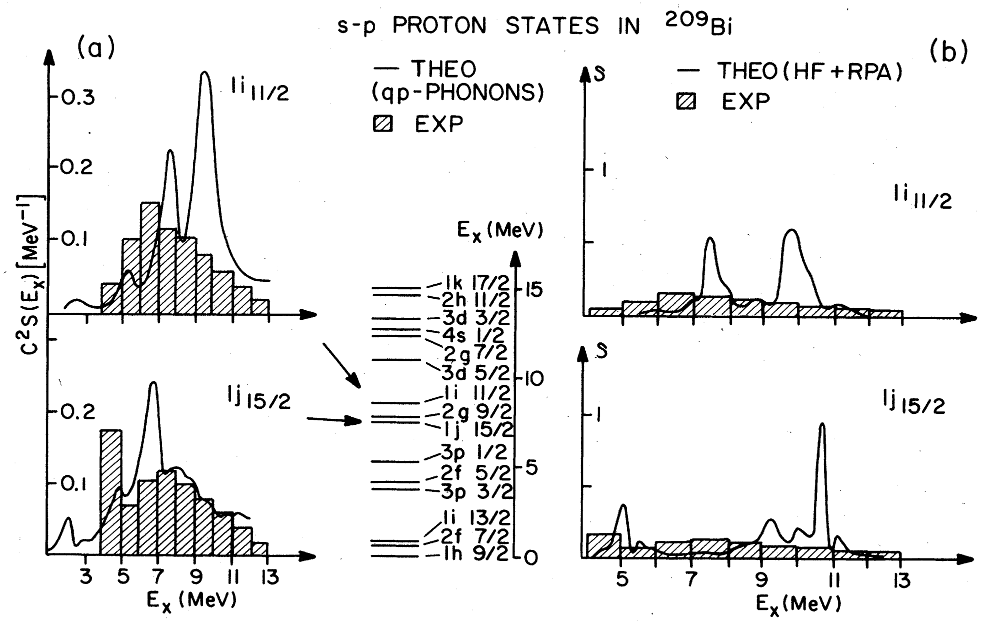


FIG. 16. (a) Comparison between theoretical strength functions (full curved) from the quasiparticle-phonon coupling nuclear model (Ref. 27) and experimental distributions (hatched areas) for the high-lying $1i_{11/2}$ and $1j_{15/2}$ subshells in $^{209}$Bi. On the right-hand side of the figure is displayed the level scheme of proton quasiparticle states calculated in a Woods-Saxon potential (Ref. 27). (b) Here the theoretical strength functions (full curve) are from the single-particle vibration coupling nuclear model (Ref. 22).

## V. SUMMARY AND CONCLUSIONS

Our empirical knowledge of the single-particle strength functions in medium-heavy weight nuclei has been greatly enhanced by the observation of new high-lying modes in proton stripping reactions. The investigation of a large excitation energy range with adequate energy resolution and good statistics has allowed a rather complete description of both the low- and high-lying proton states in $^{117}$Sb, $^{145}$Eu, and $^{209}$Bi. The ($\alpha$,t) reaction appears to be a good tool for nuclear structure studies of high-spin orbitals. The large enhancement of cross sections observed between 5 and 15 MeV excitation energy in the three nuclei investigated here arise from proton stripping to high-spin outer subshells and display striking similarities with those observed in the early experiments on deeply-bound neutron-hole states.[4,9]

Two theoretical approaches were rather successful in reproducing the empirical systematics. The Dubna group[5,27] using the quasiparticle-phonon coupling model has reached a good quantitative understanding of the damping of such nuclear excitations. In general, centroid energies, widths, total amount of strengths, and overlap between different subshells are in reasonable agreement with experiments. However, the detailed structure of the predicted strength distributions displays rather narrow concentration of strengths which are not observed experimentally. On the other hand, a theoretical model that has found considerable success, is based on a damping mechanism in which the simple excitations mix with the surface vibrations.[6,7,22] A self-consistent mixing between the single-particle motion (calculated with the Hartree-Fock field) and vibrations from RPA calculations could be achieved. The theoretical predictions are made for both the low-lying and high-lying proton subshells with practically no free parameters.

At the qualitative level, the agreement with the empirical data is rather good. However, at the quantitative level, the predicted strength distributions are not damped enough (often by a factor of 2), a general feature already noted in the case of inner-hole strength functions.[5,7] From the experimental side, one foresees the necessity of exclusive experiments, such as gamma or particle decay of high-lying states, in order to avoid the problem of the background substraction and to gain insight on the damping mechanisms.

We would like to thank Dr. Ch. Stoyanov for many stimulating discussions and Dr. N. Van Giai for communications of his results prior to publication. One of us (C.P.M.) would like to acknowledge the CONICET (Argentina) for their financial support during the course of this work.

[1]R. L. McGrath, N. Cue, W. R. Hering, L. L. Lee, Jr., B. L. Liebler, and Z. Vager, Phys. Rev. Lett. **25**, 663 (1970).

[2]S. Gales, in *Proceedings of the International Symposium on Highly Excited States in Nuclear Reactions, Osaka, Japan, 1980,* edited by H. Ikegami and M. Muraoka (RCNP, Osaka, 1980), p. 473.

[3]R. H. Siemssen, J. Phys. Soc. Jpn. **44**, 137 (1978).

[4]S. Gales, in Proceedings of International Conference on Nuclear Structure, Berkeley, 1980, Nucl. Phys. **A354**, 193C (1981).

[5]V. G. Soloviev, Ch. Stoyanov, and A. I. Vdovin, Nucl. Phys. **A342**, 261 (1980).
[6]G. Bertsch, P. F. Bortignon, R. A. Broglia, and C. H. Dasso, Phys. Lett. **80B**, 167 (1979); Rev. Mod. Phys. **55**, 287 (1983).
[7]N. Van Giai and V. Bernard, see Ref. 2, p. 682.
[8]S. Gales, C. P. Massolo, S. Fortier, E. Gerlic, J. Guillot, E. Hourani, J. M. Maison, J. P. Schapira, and B. Zwieglinski, Phys. Rev. Lett. **48**, 1593 (1982).
[9]M. Sakai and K. Kubo, Nucl. Phys. **A185**, 217 (1972); S. Y. Van der Werf, B. R. Kooistra, W. H. A. Hesselink, F. Iachello, L. W. Put, and R. H. Siemssen, Phys. Rev. Lett. **33**, 712 (1974); E. Gerlic, J. Källne, H. Langevin-Joliot, J. Van de Wiele, and G. Duhamel, Phys. Lett. **57B**, 338 (1975); E. Gerlic, G. Berrier-Rosin, G. Duhamel, S. Gales, E. Hourani, H. Langevin-Joliot, M. Vergnes, and J. Van de Wiele, Phys. Rev. C **21**, 124 (1980).
[10]A. H. Wapstra and K. Bos, At. Data Nucl. Data Tables **19**, 215 (1977).
[11]R. L. Auble, Nucl. Data Sheets **B25**, 315 (1978), $A=117$, and references therein.
[12]J. K. Tuli, Nucl. Data Sheets **B29**, 523 (1980), $A=145$, and references therein.
[13]M. J. Martin, Nucl. Data Sheets **B22**, 545 (1977), $A=209$, and references therein.
[14]R. Perry, A. Nadasen, D. L. Hendrie, P. G. Roos, and N. S. Chant, Phys. Rev. C **24**, 1471 (1981).
[15]P. D. Kunz, University of Colorado, computer code DWUCK (unpublished).
[16]N. S. Chant and J. N. Craig, Phys. Rev. C **14**, 1763 (1976).
[17]E. Friedman, A. Moalem, D. Suraqui, and S. Mordechai, Phys. Rev. C **15**, 1604 (1977).
[18]T. I. Ishimatsu, K. Yagi, H. Ohmura, Y. Nakajima, T. Nakagawa, and H. Orihara, Nucl. Phys. **A104**, 481 (1967).
[19]M. Beiner and R. J. Lombard, Ann. Phys. (N.Y.) **86**, 262 (1974); and (private communication).
[20]B. H. Wildenthal, E. Neuman, and R. L. Auble, Phys. Rev. C **3**, 1199 (1971).
[21]B. A. Brown, S. E. Massen, J. I. Escudero, P. E. Hodgson, G. Madurga, and J. Vinas, J. Phys. G **9**, 423 (1983).
[22]N. Van Giai and Pham Van Thieu (unpublished).
[23]J. R. Wu, C. C. Chang, and H. D. Holmgren, Phys. Rev. Lett. **40**, 1013 (1978).
[24]A. Budzanowski, G. Bauer, C. Alderliesten, J. Bojowald, C. Mayer-Boricke, W. Oelert, P. Turck, F. Rosel, and D. Trautmann, Phys. Rev. Lett. **41**, 635 (1978).
[25]R. Serber, Phys. Rev. **72**, 1008 (1947).
[26]N. Matsuoka, A. Shimizu, K. Hosono, T. Saito, H. Sakaguchi, A. Goto, M. Kondo, and F. Ohtani, Nucl. Phys. **A311**, 173 (1978).
[27]Ch. Stoyanov and A. I. Vdovin, Phys. Lett. **B130**, 134 (1983); and (private communication).
[28]C. M. Vincent and H. T. Fortune, Phys. Rev. C **2**, 782 (1970).
[29]U. Strohbusch, H. J. Korner, G. C. Morrison, and J. P. Schiffer, Phys. Rev. Lett. **28**, 47 (1972).